Nuclear Engineering and Technology 54 (2022) 3429–3439

Contents lists available at ScienceDirect

Nuclear Engineering and Technology

journal homepage: www.elsevier.com/locate/net

Original Article

Validation of MCS code for shielding calculation using SINBAD

XiaoYong Feng [a], Peng Zhang [b], Hyunsuk Lee [c], Deokjung Lee [c], Hyun Chul Lee [a, *]

[a] School of Mechanical Engineering, Pusan National University, 2, Busandaehak-ro 63beon-gil, Geumjeong-gu. Busan, 46241, South Korea
[b] Graduate School of Artificial Intelligence, Korea Advanced Institute of Science and Technology, 291 Daehak-ro, Yuseong-gu, Daejeon, 34141, South Korea
[c] Department of Nuclear Engineering, Ulsan National Institute of Science and Technology, 50 UNIST-gil, Ulsan, 44919, South Korea

ARTICLE INFO

Article history:
Received 31 December 2021
Received in revised form
22 February 2022
Accepted 21 March 2022
Available online 25 March 2022

Keywords:
MCS code
SINBAD
Shielding
Verification

ABSTRACT

The MCS code is a computer code developed by the Ulsan National Institute of Science and Technology (UNIST) for simulation and calculation of nuclear reactor systems based on the Monte Carlo method. The code is currently used to solve two main types of reactor physics problems, namely, criticality problems and radiation shielding problems. In this paper, the radiation shielding capability of the MCS code is validated by simulating some selected SINBAD (Shielding Integral Benchmark Archive and Database) experiments. The whole validation was performed in two ways. Firstly, the functionality and computational rationality of the MCS code was verified by comparing the simulation results with those of MCNP code. Secondly, the validity and computational accuracy of the MCS code was confirmed by comparing the simulation results with the experimental results of SINBAD. The simulation results of the MCS code are highly consistent with the those of the MCNP code, and they are within the 2σ error bound of the experiment results. It shows that the calculation results of the MCS code are reliable when simulating the radiation shielding problems.

1. Introduction

The MCS code developed by the Ulsan National Institute of Science and Technology (UNIST) is a Monte Carlo particle transport code for large-scale power reactor analysis [1]. The most outstanding benefit of the MCS code is its high computational efficiency compared to other Monte Carlo codes. MCS reduced computing time by more than 12 times and reduced the memory requirement by more than 4 times compared to the MCNP code [2]. MCS is currently used to solve two major classes of problems related to nuclear reactor physics: (a)Criticality problems with or without burnup calculation, coupled or uncoupled with external physics codes such as fuel performance code and/or thermal hydraulics code. (b)Radiometric shielding problems such as propagation of fixed sources in multiplicative or non-multiplicative medium.

The verification and validation (V&V) of the MCS code is now particularly important because it affects the final availability of the MCS code for extensive practical applications. This study aims to verify the computational accuracy of the MCS code when solving the shielding problems. In this paper, selected SINBAD experiments [3] are used to verify the MCS code. The functionality and reasonability of the MCS code for shielding calculation are verified by comparison with the MCNP code and the reliability of the MCS code solution is confirmed by comparison with the experimental results.

To complete this V&V work, seven experiments are selected from the SINBAD experiments. They include fission reactor experiments, fusion simulation experiments and particle accelerator shielding experiments. The validation process has been conducted with MCS v1.0 and MCNP v6.0 using the nuclide cross-section data library, either ENDF/B-VIII.0 or FENDL3.1, depending on the specific experimental setup.

2. Introduction of the experiments

SINBAD is widely used as a benchmark for V&V of various shielding codes. Table 1 lists the seven experimental models selected for the V&V process. Reference 2 provides more detailed experimental data and input information for the MCNP code. All the measurement uncertainties are assumed to be two standard deviations (2σ) since it is not clearly stated in the benchmark documentation.

* Corresponding author.
E-mail address: hyunchul.lee@pusan.ac.kr (H.C. Lee).

https://doi.org/10.1016/j.net.2022.03.029

Table 1
List of the selected SINBAD Experiments.

Benchmark No.	Name	Type
NEA-1517/83	Measurements of spatial energy distributions of neutrons and photons scattered in the air near the ground-air interface	Fission reactor experiment
NEA-1553/62	FNS/JAERI Measurement of Radiation Sky-shine with D-T Neutron Source	Fusion simulation experiment
NEA-1553/45	Collection of experimental data for fusion neutronics benchmark	Particle accelerator shielding experiment
NEA-1553/72	Integral Experiment on a 60 cm-thick Graphite Cylindrical Assembly	
NEA-1553/46	TUD Iron Slab Benchmark Experiment	
NEA-1553/70	TUD/FNG measurement of neutron and photon flux spectra in the FNG silicon carbide benchmark assembly	
NEA-1553/47	TUD/FNG measurement of neutron and photon flux spectra in the FNG tungsten assembly	

2.1. NEA-1517/83 Benchmark

The experiment was established by the Kazakh National Nuclear Center Kurchatov Institute of Atomic Energy (IAE NNC RK). The experimental model is the RA research reactor [4]. As shown in Fig. 1, sectional view of the reactor, a shielding plug is installed above the reactor, which consists of a 20 mm thick steel plate and an 850 mm thick concrete plug. The position of the detector in this experiment was 1 m above the ground level, and in-situ dose measurements were performed at distances of 50, 100, 200, 300, 400, 500, 600, 800, and 1000 m from the reactor axis. The data tested in the experiment include neutron flux, neutron dose rate, and neutron spectrum. The power of the reactor during the experiment was 300 kW.

The core of the RA research reactor is a fission radiation source with a 700 mm high, 297 mm diameter core consisting of 37 air-cooled fuel assemblies and highly enriched fuel made from uranium carbide. The primary material of the moderator is zirconium hydride, with a diameter of 339 mm, of which 372 holes with a diameter of 3 mm are used for cooling. The reflector layer on the side of the reactor consists of a 102 mm thick beryllium blocks, a 16 mm steel vessel, and a 180 mm thick graphite blocks. The core and the reflector are surrounded by a biological shield of heavy serpentine concrete 1100–1400 mm thick, surrounded by steel material outside the shield, about 350 mm thick.

2.2. NEA-1553/62 Benchmark

The experiment was conducted at the Tokamak Fusion Test Reactor (TFTR) in the Princeton Plasma Physics Laboratory. The experimental setup is housed in a large laboratory with a square of 15×15 m^2 and a height of 9.1 m. The main structure of the laboratory is concrete with a thickness of 1.15 m and 2.0 m at the top and the side wall, respectively. To reduce the neutron scattering from the ground, the floor structure of the room is made of an iron fence. The D-T source is 1.8 m above the ground, 5.5 m from the southern wall, and 2.75 m from the western wall. There is a square hole at the top of the lab measuring 0.9×0.9 m^2. This hole is usually closed with a concrete plug, but it is necessary to remove the concrete plug for sky irradiation experiments and replace it with a 2 mm thick stainless-steel plate only to maintain the air pressure in the laboratory. The neutron attenuation of the 2 mm stainless steel plate is negligible [5]. The main structure is shown in Fig. 2. The experimental model was simplified during the simulation process of the experiment. The iron fence structure was not constructed, and the experimental site was changed to an axisymmetric cylinder.

The main structure of the laboratory is artificial concrete, the land material is standard concrete, and the whole experiment is conducted in an air environment. The experimental facility uses a nuclear fusion D-T neutron source as the experimental source, which is generated by the FNS (Fusion Neutronics Source) particle acceleration, and the yield of the neutron source is about 1.7×10^{11} neutron/sec [6].

The experimental device is only 150 m away from the Pacific Ocean and is in a plain. Pine forests surround the north and east sides of the experimental device. The height of the pine forest is about 10 m. The neutron dose rate is measured at 20–550 m from the D-T neutron source in the northern pine forest of the experimental device. The neutron dose rate was measured at 20–140 m

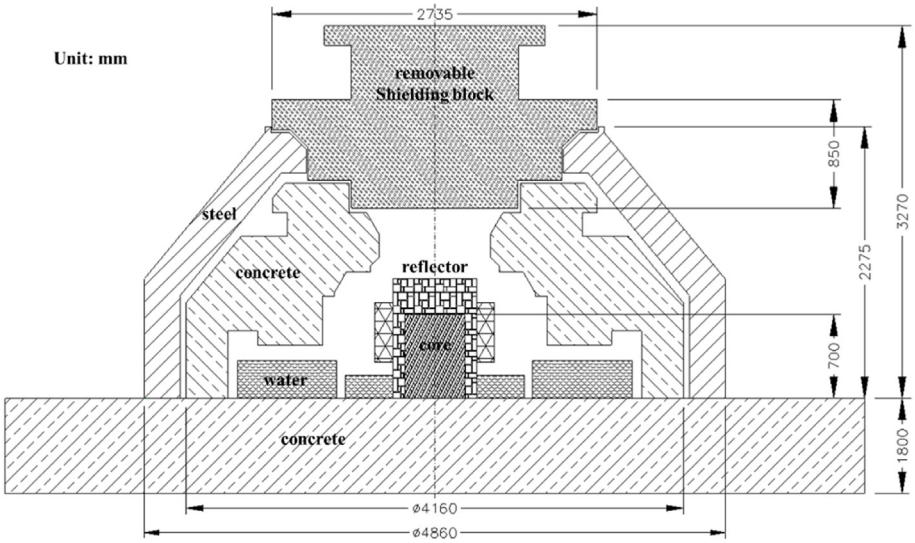

Fig. 1. RA-reactor model.

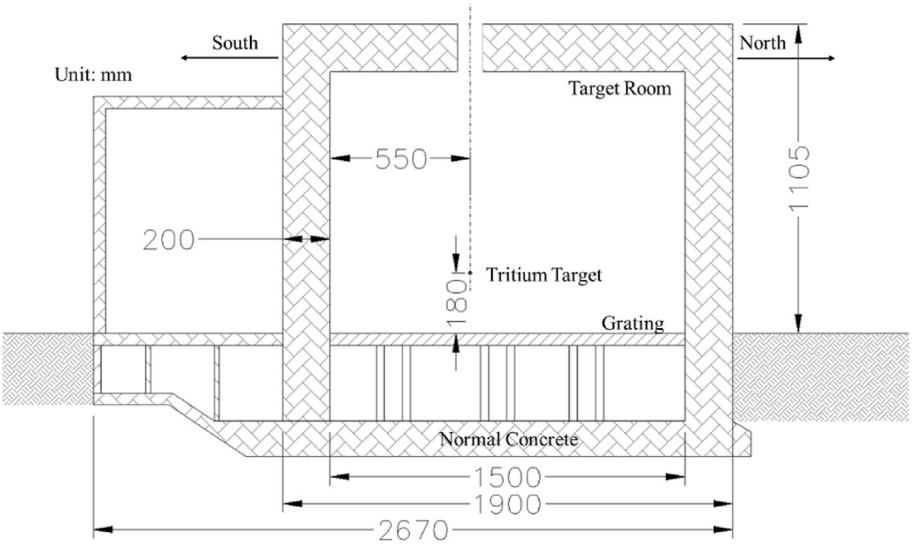

Fig. 2. TFTR model.

from the D-T neutron source on the southern highway of the experimental device, and the neutron dose rate was measured at 200, 230, and 300 m from the D-T neutron source in the southwest of the experimental device. All the measuring points use the spherical rapid eye movement counter Fuji Electric NSN10002 to measure the neutron dose rate. The uncertainty of actual measurement results is less than 20% [5].

2.3. NEA-1553/45 and NEA-1553/72 Benchmark

The FNS Benchmark experiment is a D-T nuclear fusion neutron source neutronic benchmark experiment conducted in Japan Atomic Energy Research. The floor of the experimental device is a grating structure, and the room is large enough to ignore the influence of the room structure on the test results [7,8]. The two experimental models are basically similar except for the different sizes of shielding materials and shielding structures. The neutron source is in the back of the shielding wall whose geometry is shown in Fig. 3. The shielding components are fixed in an aluminum frame, and the frame and components are installed on a steel deck. The distance between the D-T neutron source and the front surface of the module is 200 mm. Table 2 shows the detailed dimensions of the experiments.

The neutron source used in this experiment was generated by the Fusion Neutronics Source (FNS) particle accelerator and the maximum neutron production is about 3×10^{11} neutrons/s.

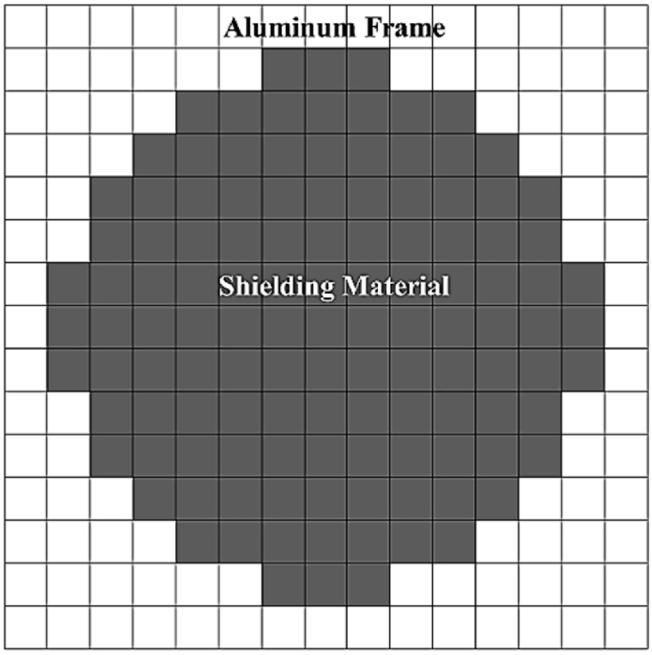

Fig. 3. FNS model front surface.

Table 2
Dimensions of the shielding structure of NEA-1553/45 and NEA-1553/72.

Experiment	Shielding Material	Effective Diameters	Thickness
NEA-1553/45	Copper	629 mm	608 mm
NEA-1553/72	Graphite	628 mm	610 mm

2.4. NEA-1553/46, NEA-1553/70, NEA-1553/47 Benchmark

The TUD experimental model was constructed by the Technische Universität Dresden (TUD) team. The shielding materials for the three experimental models are iron, SiC, and tungsten, respectively.

The experimental model of iron shielding is shown in Fig. 4. Q and D in the figure represent the position of the D-T neutron source, the position of the neutron detector, respectively [9–12]. Table 3 shows the detailed dimensions of the experiments.

The dimensions and the position of the collimator are not given in the benchmark file, and there are geometric errors in the MCNP input information provided in the benchmark. Therefore, based on the image and the MCNP input information, the dimensions and position of the collimator were redefined as shown in Fig. 4.

The components of the SiC shielding experiment and the tungsten shielding experiment are shown in Fig. 5. The geometry of the two experimental models is similar, but there are certain size differences. The dimensions of the SiC assembly are $45.7 \times 45.7 \times 71.1$ cm^3 [13]. The dimensions of the tungsten assembly are $47 \times 47 \times 49$ cm^3 [14]. The position of the FNG neutron source is 5.3 cm from the surface of the experimental component [15]. The NE213 scintillation spectrometer was used to measure the

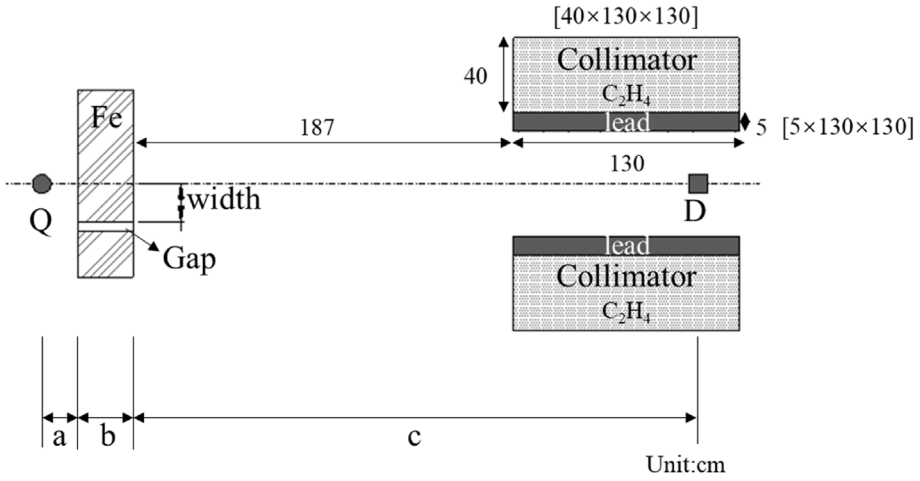

Fig. 4. NEA-1553/46 model.

Table 3
Dimensions of the shielding structure of NEA-1553/46.

Model	Gap [cm]	Width [cm]	Area [cm^2]	a [cm]	b [cm]	c [cm]
A0	0	0	100 × 100	19	30	300
A1	5	10				
A2	5	20				

Table 4
Dimensions of the shielding structure of NEA-1553/70, NEA-1553/47.

Experiment	Shielding Material	Area [cm^2]	T [cm]	a [cm]	b [cm]	c [cm]	d [cm]
NEA-1553/70	SiC	45.7 × 45.7	71.1	12.70	27.94	43.18	58.42
NEA-1553/47	Tungsten	47.0 × 47.0	49.0	5	15	25	35

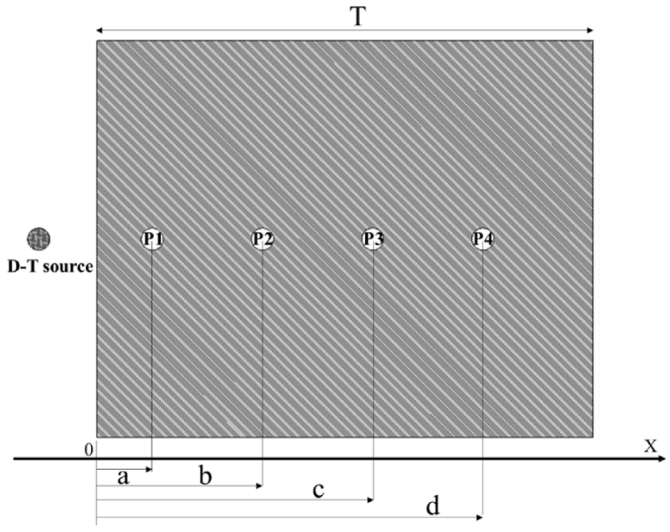

Fig. 5. TUD SiC and W model.

neutron spectrum. The detector is a cylinder with a height and diameter of 3.8 cm. The material has a mass density of 0.874 g/cm^3 and an elemental composition of 54.8 at-% H and 45.2 at-% C [16]. The detectors were arranged at four positions P1, P2, P3, and P4 (see Table 4).

The neutron source used in this experiment is a 14 MeV D-T neutron source generated by the Frascati Neutron Generator (FNG) particle accelerator [17]. A deuteron with an energy of 125 KeV was used to impact the T-Ti target in the accelerator to generate neutrons, and the accompanying alpha particles determined the intensity of the resulting D-T neutron source. The particle gas pedal operates in a pulsed mode, recording the pulse height and arrival time t (14 MeV neutrons are produced when t = 0), and the time distribution of the source is proportional to exp [-(t/1.4 ns)^2].

3. Calculation results

In this section, the simulation results of MCS code as well as the simulation results of MCNP code and the experimental data are given with an uncertainty range of ±2σ. The MCS code uses the weight window (WW) technique to reduce variance during simulation. The WW feature is composed of two steps. In the first step, optimized weights for a given tally detector of the problem is calculated. In the second step, the weights are used to perform population control of the particles through splitting and Russian roulette. The details of WW of the MCS code can be found in reference [18].

3.1. NEA-1517/83 Benchmark

Figs. 6–8 compare the simulation results of MCS and MCNP codes and the experimental data of NEA-1517/83 benchmark problem. Fig. 6(a) shows that the simulation results of thermal neutron flux

are consistent with each other, but they are much higher than the experimental data. The statistical error of the two simulation results except for those at 1000 m are small enough and they are not noticeable in the figure. The inconsistency in the thermal neutron flux is explained in the benchmark book as follow [3]: "This discrepancy results from neglect of the characteristic function of the response of the scintillation spectrometer from lithium fluoride." In contrast, the simulation results of the intermediate and fast neutron fluxes are entirely consistent with the experimental data within the error bound as shown in Fig. 6(b). The neutron dose rates agree with the experimental data as well within the experimental uncertainty as shown in Fig. 7. Fig. 8 shows the spectrums at the detector positions of 100, 200, 400, 600, 800, and 1000 m from the reactor axis. The statistical uncertainty of the simulation increases with distance and with higher neutron energy. The maximum and average bias of the MCS code results as well as the statistical and experimental errors are tabulated in Table 5. Considering the calculational and experimental uncertainties, the simulation results and the experimental data are generally consistent.

In the statistical results of the neutron spectrum, when the energy is greater than 4 MeV, there is a certain error between the simulated calculation results and the experimental results, but they are also within the range of 2σ. At the same time, when the distance of the detector increases, the simulation result is compared with the experimental result, and the error also increases slightly. From the results, the simulation results of the MCS code are consistent

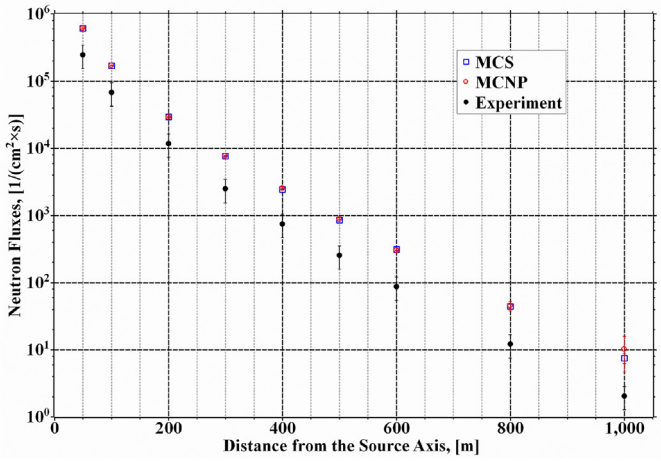

(a) Thermal (E<0.414eV) Neutron Fluxes

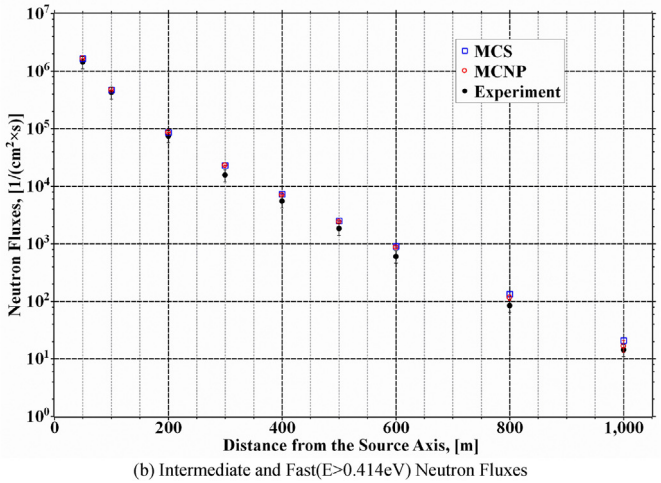

(b) Intermediate and Fast(E>0.414eV) Neutron Fluxes

Fig. 6. Neutron flux of NEA-1517/83 Benchmark.

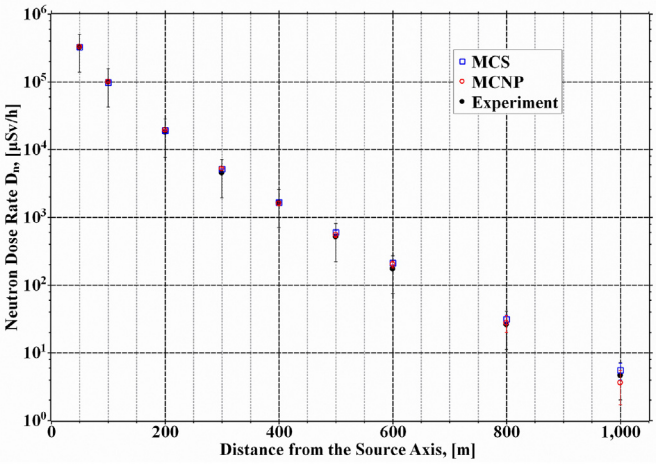

Fig. 7. Neutron dose rate of NEA-1517/83 Benchmark.

with the simulation results of the MCNP code. Compared with the experimental results, the error range is within the range of 2σ, and the simulation results are within the confidence interval.

3.2. NEA-1553/62 Benchmark

As shown in Fig. 9, the simulation results of the MCS code and the MCNP code are consistent, and they are within the confidence interval of the experimental data. Compared with the experimental results, the simulation results show some error only near the source. It is ascribed to the fact that the laboratory room was modeled as a cylinder with a source on its axis while the actual room is a cube with a source biased toward the western and southern walls.

3.3. NEA-1553/45 and NEA-1553/72 Benchmark

Some simplifications were introduced when building simulation models for these two benchmark experiments. A point source at the actual source location was modeled without modeling the FNS particle accelerator and only shielding blocks were modeled by ignoring the aluminum frame.

Fig. 10 shows the results for copper shielding blocks. The simulation results of the MCS code and the MCNP code agree well for entire energy range and for all distances. Though there is some discrepancy between the simulation results and the experimental data in the energy range of 0.1–1.0 MeV at 76 m and in the energy range of 1–4 MeV at 532 mm, the simulation results are consistent with the experimental data within their uncertainty level for other cases.

Fig. 11 shows the results for graphite shielding blocks. In the actual experiment, when the energy is lower than 1 MeV, the results are not reliable [11] due to systematic and measurement errors, so only the result above 1 MeV are shown in Fig. 11. It can be seen from the figure that the simulation calculation results of the MCS code and the MCNP code maintain a high degree of consistency. In the high-energy region where the neutron flux rapidly increases and decreases as the energy increases, the simulation results and the experimental data show a large difference. However, in all other energy domains, simulation results and experimental data are consistent.

3.4. NEA-1553/46, NEA-1553/70, NEA-1553/47 Benchmark

Since the NEA-1553/46 Benchmark file did not provide detailed

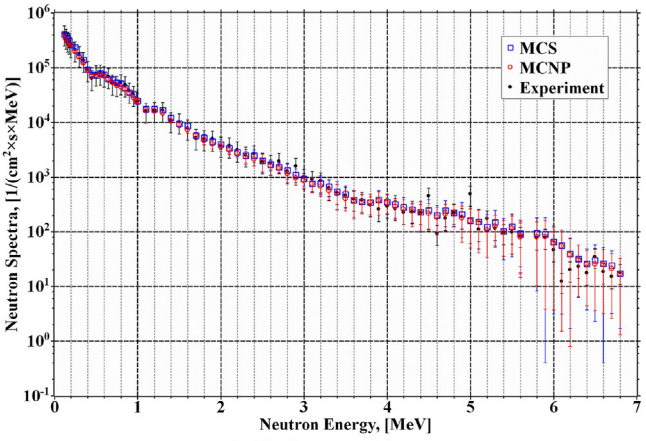

(a) The detector at **100 m**

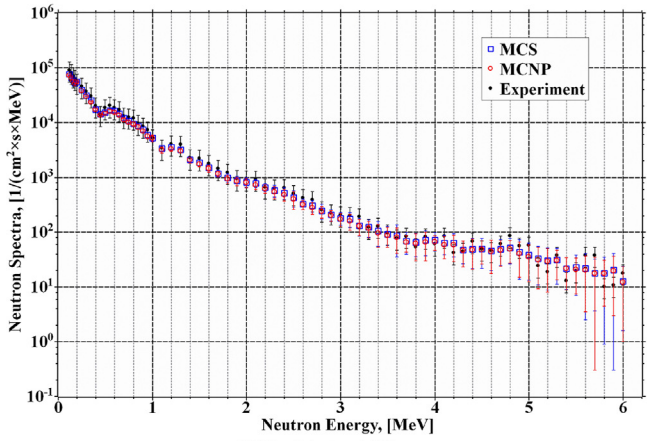

(b) The detector at **200 m**

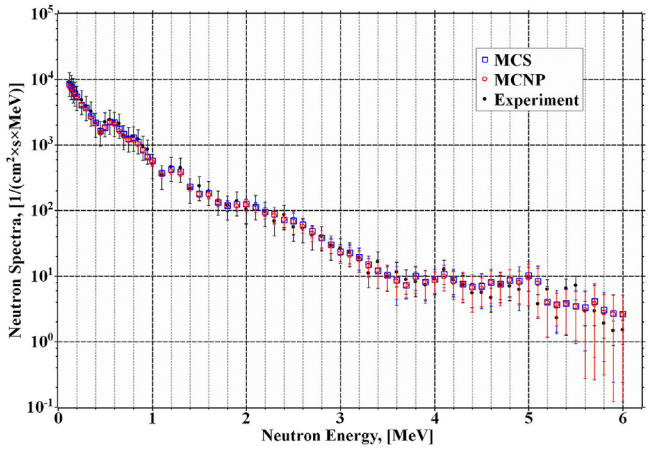

(c) The detector at **400 m**

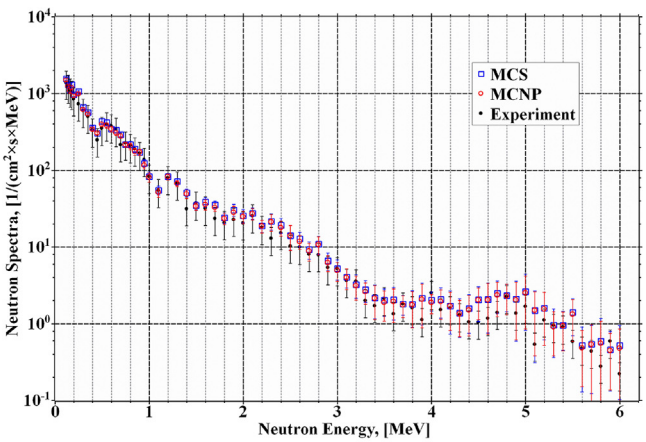

(d) The detector at **600 m**

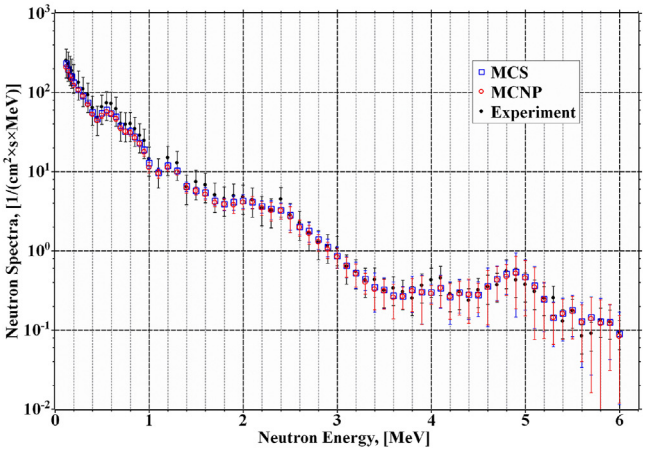

(e) The detector at **800 m**

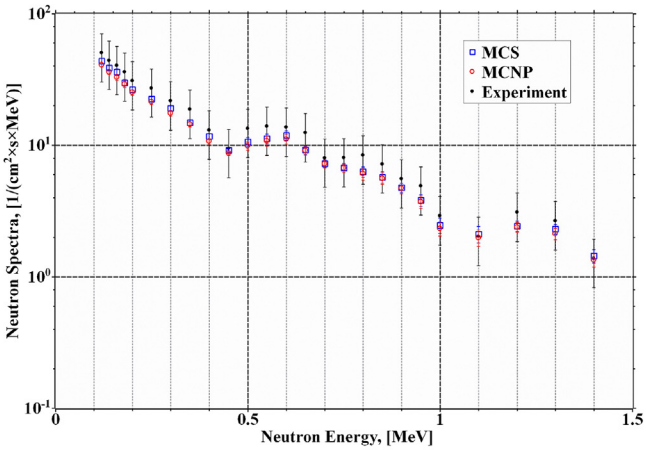

(f) The detector at **1000 m**

Fig. 8. Neutron spectra of NEA-1517/83 Benchmark.

Table 5
The bias and the statistical error of NEA-1517/83.

Tally		Bias of MCS[a] [%]		Mean of Std. Dev. [%]	
		Maximum	Average	MCS	Exp.
Thermal Neutron Fluxes [1/(cm^2·s)]		397.19	230.39	2.00	19
Fast Neutron Fluxes [1/(cm^2·s)]		44.96	26.49	1.72	12
Neutron Dose Rate [μSv/h]		22.49	8.56	2.34	19
Neutron Spectra [1/(cm^2·s·MeV)]	100[m]	348.01	21.96	19.32	20
	200[m]	84.37	21.41	15.90	20
	400[m]	108.47	20.04	15.91	20
	600[m]	177.59	30.27	15.23	20
	800[m]	61.18	15.85	15.38	20
	1000[m]	53.04	16.44	3.77	20

[a] $|MCS - Exp.|/Exp.$

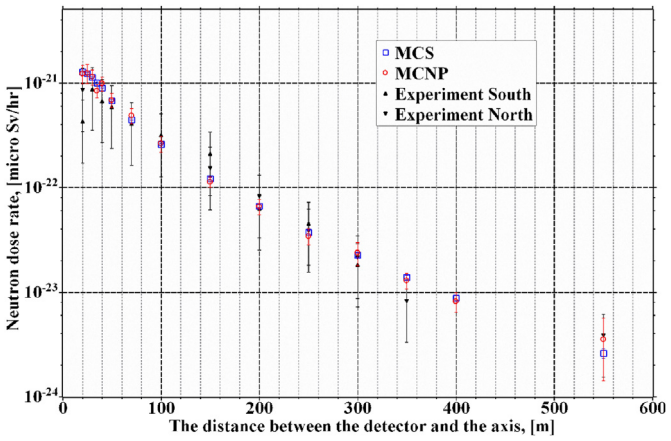

Fig. 9. Neutron dose rate of NEA-1553/62 Benchmark.

size data of the experimental model, the model was only restored based on the picture information provided by the reference file. Although the model established by simulation has been established as close as possible to the actual model, there will still be a particular deviation between the size of the model used in the simulation calculation and the size of the actual experimental model, which may lead to errors between the final simulation results and the experimental results.

Fig. 12 shows a comparison of the results for the NEA-1553/46 benchmark. It can be seen from the results that although the experimental model was changed by adding gaps in the shield, this change in dimensions did not affect the experimental results.

The calculated results of the MCS code and the MCNP code are consistent. When the energy is in the range of 8–12 MeV, the calculated results are smaller than the experimental results, which is the same information provided by the Benchmark book [14], but the reason is unclear. When the energy is greater than

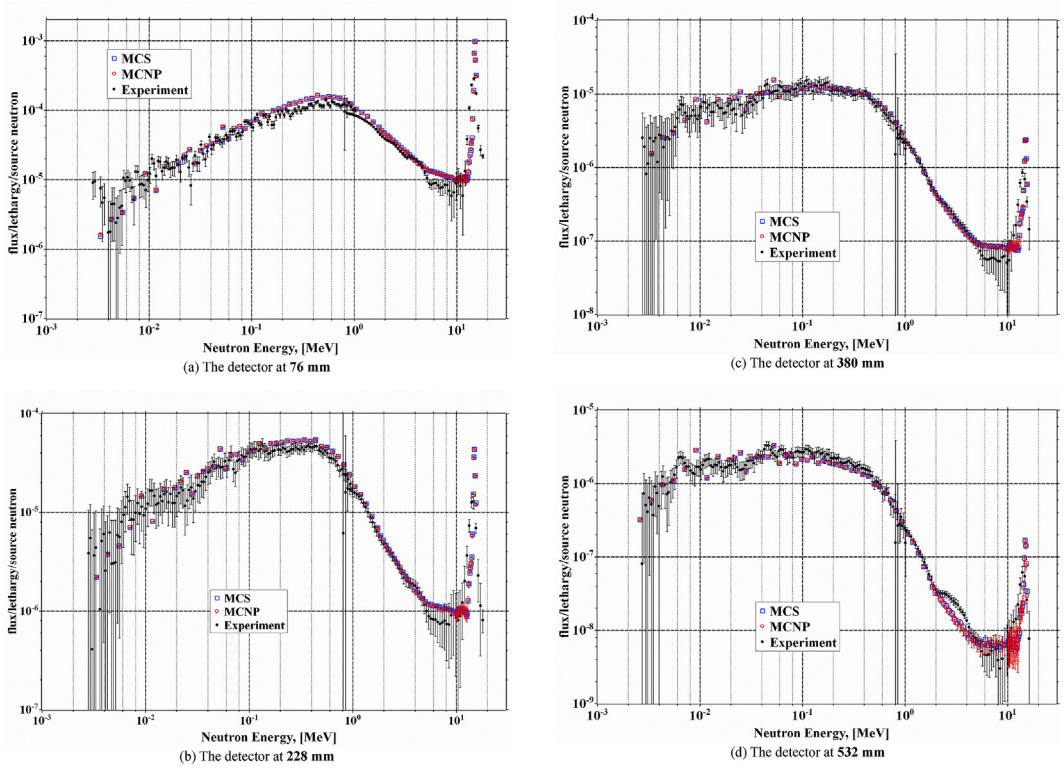

Fig. 10. Neutron spectra of NEA-1553/45 Benchmark.

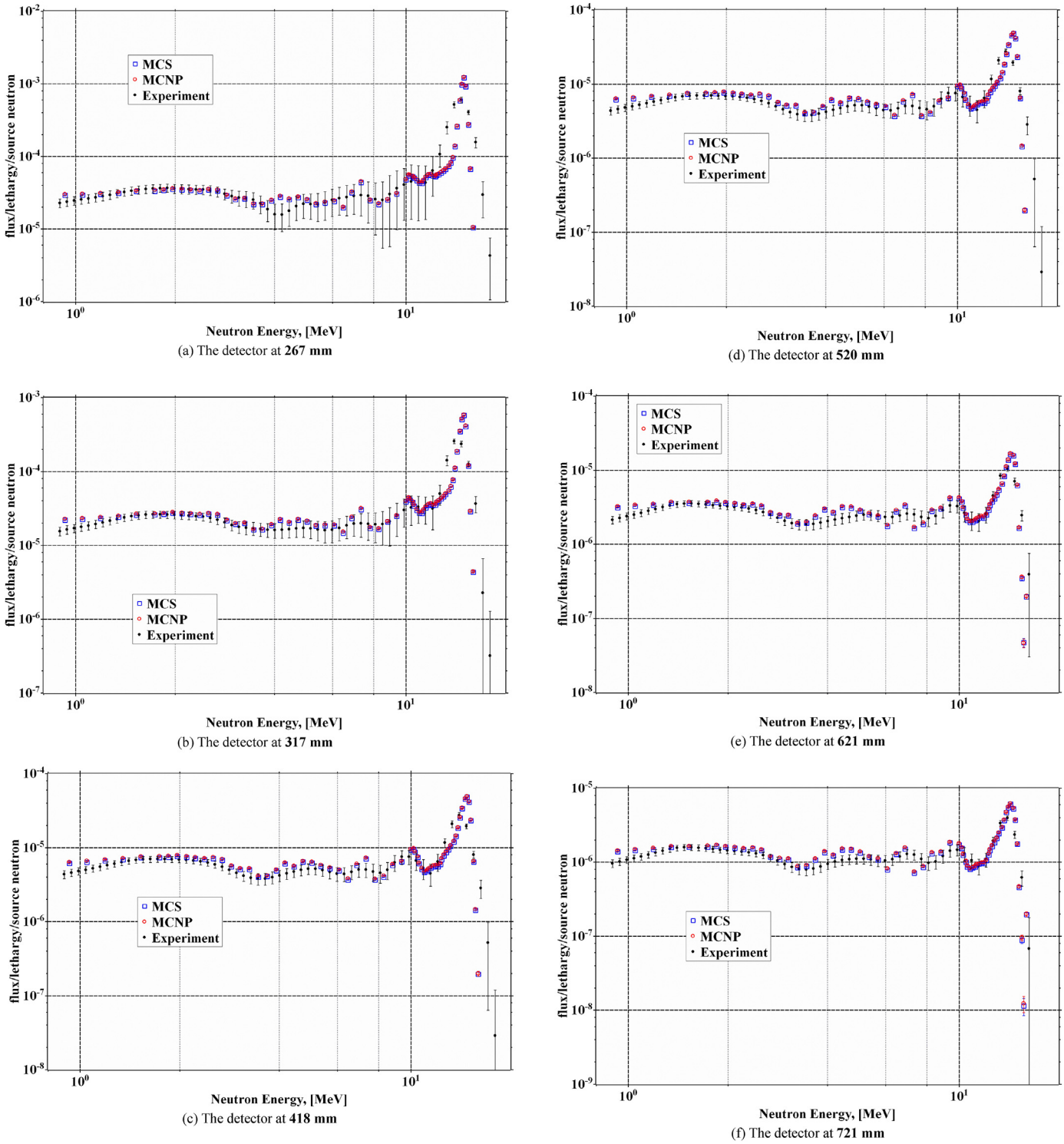

(a) The detector at **267 mm**

(d) The detector at **520 mm**

(b) The detector at **317 mm**

(e) The detector at **621 mm**

(c) The detector at **418 mm**

(f) The detector at **721 mm**

Fig. 11. Neutron spectra of NEA-1553/72 Benchmark.

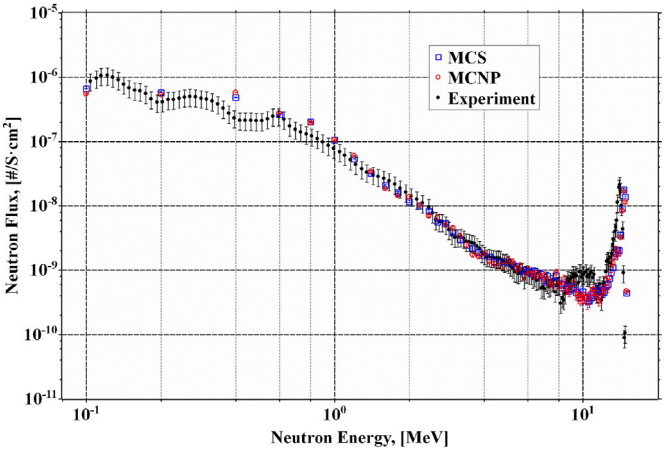

(a) **A0** Model

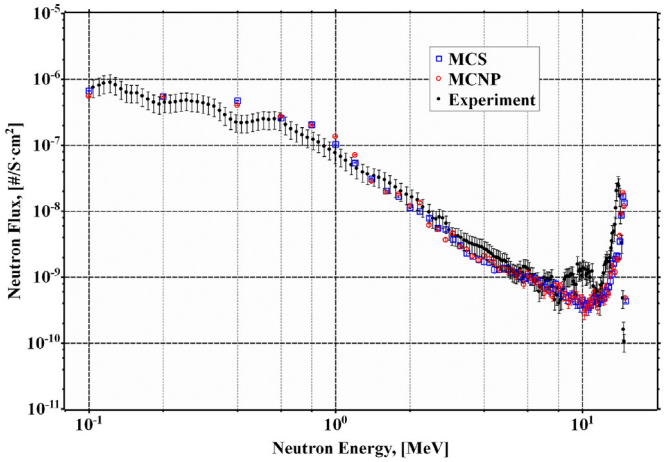

(b) **A1** Model

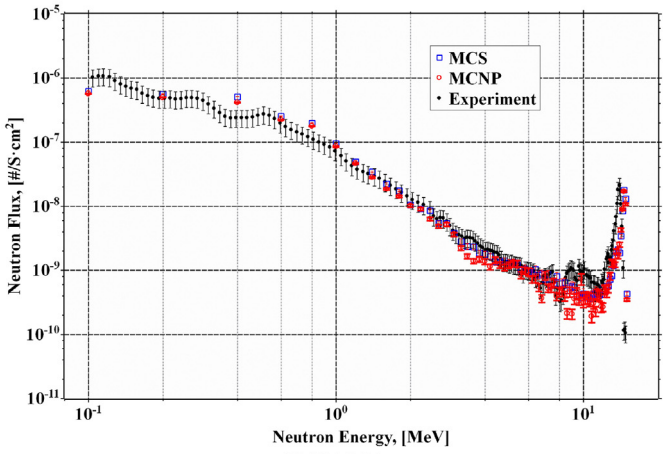

(c) **A2** Model

Fig. 12. Neutron flux of NEA-1553/46 Benchmark.

12 MeV, the simulated results are shifted by 500 keV positively. This error may be caused by the size and shape differences with the actual model due to insufficient data when building the model.

Fig. 13 compares the results for the NEA-1553/70 benchmark. From the results, it can be found that the simulation results of the MCS code are consistent with those of the MCNP code, but when the detector position is at the P1 position (Fig. 13(a)), the simulation result is much larger than the experimental result. The reason for is not clear, but it is the same as the result given in the benchmark document. The simulation results at the other three positions are basically consistent with the experimental results, and the error range is within 2σ.

Fig. 14 compares the results for the NEA-1553/47 benchmark. Similarly, the simulation results of the MCS code is consistent with those of the MCNP code. The simulation results are within the error bound (2σ) of experimental results except for some energy range around 13–14 MeV. Overall, the simulation results are consistent with the experimental results.

4. Conclusion

In this work, the MCS code was verified and validated against the MCNP code and experimental results of some benchmarks such as NEA-1517/83, NEA-1553/62, NEA-1553/45, NEA-1553/72, NEA-1553/46, NEA-1553/70, and NEA-1553/47. Benchmark models for MCS code were developed for MCS Monte-Carlo simulation and the results of the MCS code were compared with those of the MCNP code and the experimental results provided in the benchmark book. The MCNP simulation was performed using the input provided in the benchmark book with some error corrections.

In the NEA-1517/83 benchmark simulation calculation, the simulation results are consistent with the experimental results except for the thermal energy range due to neglecting characteristic function of the response of the scintillation spectrometer from lithium fluoride. In the NEA-1553/62 benchmark simulation calculation, there is a small amount of deviation in the simulation results near the source point due to simplification of geometrical model, but all the other simulation results are within the confidence interval. In the NEA-1553/45 and NEA-1553/72 benchmark simulation calculations, the simulation results are consistent with the experimental results except for some energy ranges. In the NEA-1553/46 benchmark simulation calculation, the simulation results smaller than the experimental data in the energy range of 8–12 MeV. In the NEA-1553/70 and NEA-1553/47 benchmark simulation calculations, the simulation result curve is consistent with the experimental result curve, but at the P1 position, the simulation result is larger than the experimental result.

In summary, when the simulation environment of the MCS code is consistent with the MCNP code, the computational results maintain a high degree of consistency, indicating that there is no problem with the computational power of the MCS code in solving the shielding problem. When the MCS simulation results are compared with the experimental results, specific errors do exist. However, after excluding unexpected factors in the experiments, the MCS simulation results agree with the experimental results, and the simulation results are within the confidence interval. The results show that the computational accuracy of the MCS code is reliable among several experimental models that have been conducted.

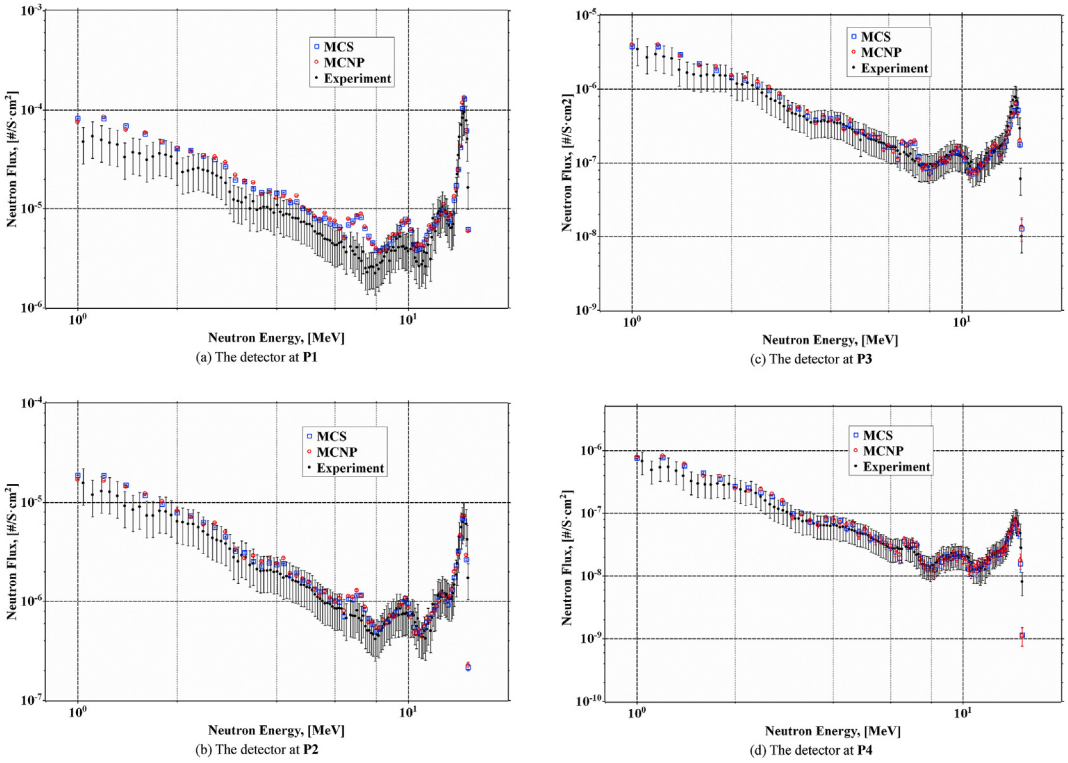

Fig. 13. Neutron spectra of NEA-1553/70 Benchmark.

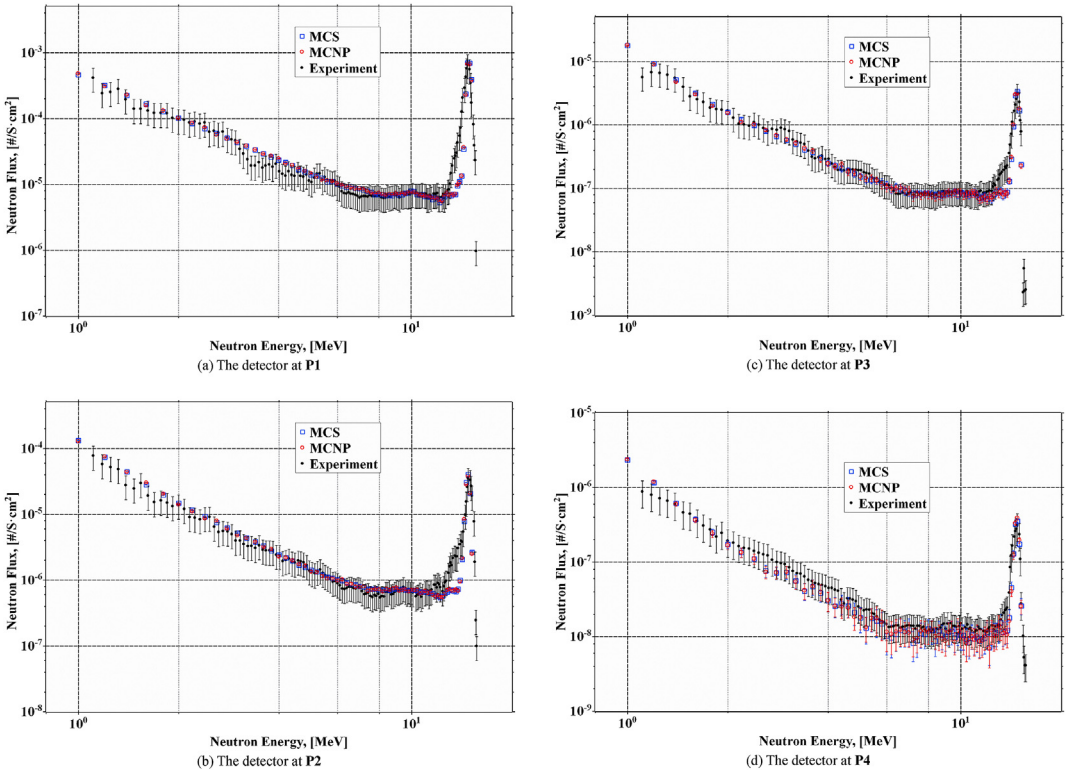

Fig. 14. Neutron spectra of NEA-1553/47 Benchmark.

Declaration of competing interest

The authors declare that they have no known competing financial interests or personal relationships that could have appeared to influence the work reported in this paper.

Acknowledgements

This work was supported by the National Research Foundation of Korea (NRF) grant funded by the Korea government (2019R1A2C2089962).

References

[1] H. Lee, W. Kim, P. Zhang, A. Khassenov, Y. Jo, D. Lee, Development Status of Monte Carlo Code at UNIST, KNS Spring Meeting, Jeju, Korea, May 12-13, 2016.
[2] Vutheam Dos, Hyunsuk Lee, Yunki Jo, Matthieu Lemaire, Wonkyeong Kim, Sooyoung Choi, Peng Zhang, Deokjung Lee, Overcoming the challenges of Monte Carlo depletion: application to a material-testing reactor with the MCS code, Nucl. Eng. Technol. 52 (Issue 9) (September 2020) 1881–1895.
[3] I. Kodeli, E. Sartori, B. Kirk, SINBAD Shielding Benchmark Experiments Status and Planned Activities" the American Nuclear Society's 14th Biennial Topical Meeting of the Radiation Protection and Shielding Division, April 3-6, 2006. Carlsbad New Mexico, USA.
[4] Mikhail E. Netecha, et al., Experimental Study of Reactor Radiation Scattering in the Atmosphere, Research Development Institute of Power Eng, 1998, pp. 517–596.
[5] S. Yoshida, T. Nishitani, K. Ochiai, J. Kaneko, J. Hori, S. Sato, M. Yamauchi, R. Tanaka, M. Nakao, M. Wada, M. Wakisaka, I. Murata, C. Kutukake, S. Tanaka, T. Sawamura, A. Takahashi, Measurement of radiation skyshine with D-T neutron source, Fusion Eng. Des. 69 (2003) 637–641.
[6] H. Maekawa, , et al.M. J, Fusion Blanket Benchmark Experiments on a 60 Cm-Thick Lithium Oxide Cylindrical Assembly, 1986, pp. 86–182.
[7] Sub Working Group of Fusion Reactor Physics Subcommittee, Collection of Experimental Data for Fusion Neutronics Benchmark JAERI-M 94-014, February 1994.
[8] F. Maekawa, et al., Benchmarck Experiment on a Copper Slab Assembly Bombarded by D-T Neutrons JAERI-M 94-038, March 1994.
[9] H. Freiesleben, W. Hansen, D. Richter, K. Seidel, S. Unholzer, TUD experimental benchmarks of Fe nuclear data, Fusion Eng. Des. 37 (1997) 31–37.
[10] H. Freiesleben, W. Hansen, H. Klein, T. Novotny, D. Richter, R. Schwierz, K. Seidel, M. Tichy, S. Unholzer, Experimental Results of an Iron Slab Benchmark, Report Technische Universitaet Dresden", February 1995. TUD-PHY-94/2.
[11] H. Freiesleben, W. Hansen, D. Richter, K. Seidel, S. Unholzer, Experimental investigation of neutron and photon penetration and streaming through iron assemblies, Fusion Eng. Des. 28 (1995) 545–550.
[12] U. Fischer, H. Freiesleben, H. Klein, W. Mannhardt, D. Richter, D. Schmidt, K. Seidel, S. Tagesen, H. Tsige-Tamirat, S. Unholzer, H. Vonach, Y. Wu, Application of improved neutron cross-section data for Fe-56 to an integral fusion neutronics experiment, Int. Conf. on Nuclear Data for Science and Technology, Trieste (Italy) (May 19-24, 1997) 1137–1139.
[13] K. Seidel, M. Angelone, P. Batistoni, Y. Chen, U. Fischer, H. Freiesleben, C. Negoita, R.L. Perel, M. Pillon, S. Unholzer, Measurement and analysis of neutron and gamma-ray flux spectra in SiC, Fusion Eng. Des. 69 (2003) 379–383.
[14] H. Freiesleben, C. Negoita, K. Seidel, S. Unholzer, U. Fischer, D. Leichtle, M. Angelone, P. Batistoni, M. Pillon, Measurement and Analysis of Neutron and γ-ray Flux Spectra in Tungsten", Report TU Dresden, Institut für Kern-und Teilchenphysik, March 2003. TUD-IKTP/01-03.
[15] H. Freiesleben, W. Hansen, D. Richter, K. Seidel, S. Unholzer, Shield Penetration Experiments, Report Technische Universitaet Dresden, Institut fuer Kern-und Teilchenphysik, January 1995. TUD-IKTP-95/01.
[16] S. Guldbakke, H. Klein, A. Meister, J. Pulpan, U. Scheler, M. Tichy, S. Unholzer, in: H. Farrar, et al. (Eds.), Response Matrices of NE213 Scintillation Detectors for Neutrons", Reactor Dosimetry ASTM STP 1228, American Society for Testing Materials, Philadelphia, 1995, pp. 310–322.
[17] M. Angelone, M. Pillon, P. Batistoni, M. Martini, M. Martone, V. Rado, Absolute experimental and numerical calibration of the 14 MeV neutron source at the Frascati Neutron Generator, Rev. Sci. Instrum. 67 (1996) 2189.
[18] Peng Zhang, Matthieu Lemaire, Bamidele Ebiwonjumi, Wonkyeong Kim, Hyunsuk Lee, Deokjung Lee, Nhan Nguyen Trong Mai, Extension of Monte Carlo code MCS to spent fuel cask shielding analysis, Int. J. Energy Res. (15 January 2020) 8089–8101.